Asian Journal of Chemistry; Vol. 37, No. 8 (2025), 1995-2001

ASIAN JOURNAL OF CHEMISTRY

https://doi.org/10.14233/ajchem.2025.33897

Physico-Chemical Characterization and Environmental Implications of Jarosite Waste from Zinc Hydrometallurgical Processing

VASEEM AKHTAR and DINESH KULHARY*

Department of Chemistry, Career Point University, Kota-325003, India

*Corresponding author: E-mail: dinesh.kulhary@cpur.edu.in

Received: 19 April 2025; *Accepted*: 15 July 2025; *Published online*: 31 July 2025; AJC-22078

This study reports the physico-chemical properties and environmental implications of jarosite waste generated from the zinc hydrometallurgical processing. Jarosite waste samples from a major zinc processing facility were analyzed alongside soil samples from surrounding areas to assess the potential environmental impacts. Comprehensive characterization was performed using multiple analytical techniques including ICP-OES for major element analysis, ICP-MS for trace elements and heavy metals, FTIR spectroscopy, XRD and zeta potential measurements. Results revealed that the jarosite waste contains significantly increased concentrations of Fe_2O_3 (37.8-42.5%), SO_3 (20.9-26.1%) and ZnO (6.1-7.7%), with concerning levels of heavy metals including Zn (52,084-59,979 mg/kg), Pb (5,938-8,612 mg/kg) and Cd (140-237 mg/kg). XRD analysis confirmed the predominance of jarosite minerals with secondary phases of iron oxides and quartz. FTIR spectroscopy identified the characteristic sulfate stretching vibrations (1080-1190 cm^{-1}) and Fe-O bonds (510-630 cm^{-1}). Zeta potential measurements demonstrated the highly acidic nature of jarosite waste with an isoelectric point at approximately pH 3.2, significantly lower than surrounding soils (pH 5.8). Statistical analysis revealed the strong positive correlations between heavy metal concentrations and sulfate content, suggesting co-precipitation mechanisms during jarosite formation. The extreme acidity (pH 2.6-3.3) and high electrical conductivity (3.57-4.58 mS/cm) of jarosite waste present substantial environmental risks through metal leaching and acid mine drainage. This study provides critical insights into jarosite waste characteristics that can inform improved waste management strategies, remediation approaches and potential resource recovery opportunities in zinc hydrometallurgical processing.

Keywords: Jarosite waste, Zinc hydrometallurgy, Heavy metal contamination, Acid mine drainage.

INTRODUCTION

The mining and metallurgical sectors are the foundation of global economies. The metal extraction sector, while vital for the economy, generates significant quantities of waste that pose environmental challenges [1]. Especially, the wastes from mining and metallurgical activities are notorious and contains potentially toxic elements (PTEs). Of these, jarosite waste generated from zinc hydrometallurgical processing is a major environmental concern due to its acidity and potentially high heavy metal concentrations [2]. The Mewar region of India hosts several prominent zinc smelting operations [3]. Zinc smelting company is a leading integrated producer of zinc, lead and silver in India.

A common method used in the hydrometallurgical zinc production to remove impurities, particularly iron, from process solution is to precipitate jarosite [4,5]. Jarosite, a basic hydrous sulfate of potassium and iron [$KFe_3(SO_4)_2(OH)_6$], forms as a precipitate during the iron removal stage of zinc hydrometallurgy [6]. Nevertheless, this process leads to the co-precipitation of other heavy metals such as zinc, lead, cadmium and arsenic, which may turn the waste into an environmental hazard, resulting in its classification as hazardous in various countries including China and European countries [2].

Several studies [7-9] have documented potential impact of jarosite waste on surrounding soils and water bodies. Pérez-López *et al.* [10] showed that jarosite waste can contaminate surrounding soils by dust dispersion and migration of leachate. According to Navarro *et al.* [11], the weathering of jarosite waste deposits is responsible for elevated concentrations of heavy metals in soils and sediments of a zinc processing facility. Likewise, significant metal contamination in groundwater adjacent

to jarosite waste disposal sites is also reported [12]. Jarosite waste's environmental impact is complex and highly dependent over its mineralogy. Jarosite is stabilized in the form of jarofix at jarosite waste industries by treating with lime and cement and disposed in lined jarofix disposal yards [13] as an attempt to mitigate its environmental impact.

Comprehensive understanding of mineralogical properties of such industrial waste materials in comparison to natural soil systems is required for management and potential utilization of such industrial waste materials [14]. This will not only provide the potential environmental mobility of heavy metals contained in the waste, but will also guide the development of appropriate waste management strategies. Although, little research has been carried out on the comparative mineralogy of the jarosite waste from jarosite waste industries and the surrounding soil. The specific objectives of this study are to conduct a comprehensive comparative analysis of mineralogical properties between normal soil and jarosite waste material from jarosite waste industries, to assess the environmental mobility potential of heavy metals contained in the jarosite waste through mineralogical characterization and to provide the scientific insights that will guide the development of appropriate waste management strategies for the jarosite waste materials.

EXPERIMENTAL

Study area: Jarosite waste industries located in Mewar region, India. The facility is located in a semi-arid region with hot summer and cold winters and limited rainfall during the monsoon season mainly. The landscape is of undulating terrain with sparse vegetation typical of the semi-arid zones of northwestern India. The bedrock is for the most part precambrian metamorphic and igneous rocks such as schists, phyllites, quartzites and granites. The geological formations of these contain large zinc lead mineral deposits that are being exploited for metal extraction and hence the establishment of zinc smelter.

Sample collection: Sampling was done during the post monsoon period (October-November, 2024) so as to minimize seasonal variations. Samples of the soil in the vicinity of the zinc smelter plant. were collected. Locations were chosen to represent natural soil conditions unaffected by the industrial activities and locations directly affected by the waste disposal. After a systematic grid pattern was followed; 5 subsamples were taken from each sampling point and homogenized to prepare a composite sample. The samples were air dried at room temperature, disaggregated by pestle and mortar and passed through a 2 mm sieve to remove coarse fragments. The < 2 mm fraction was homogenized and stored in airtight containers for analysis at a later time. Waste samples of jarosite were collected from the secured landfill facility at zinc smelter plant. Direct sampling of fresh jarosite waste was obtained from the production process before the stabilization treatment.

Physical analysis

Colour and texture: Soil colour was determined using Munsell Soil Colour Charts under standardized daylight conditions. Texture analysis was performed using the hydrometer method following organic matter oxidation with 30% H_2O_2 and dispersion with 5% sodium hexametaphosphate. The sand (50-2000 μm), silt (2-50 μm) and clay (< 2 μm) fractions were quantified using Stokes' law, with results classified according to the USDA soil texture triangle.

Bulk density and porosity: The core method was used to determine bulk density. Stainless steel cylinders of known volume (100 mL) were used to collect the undisturbed soil samples. Dry mass was recorded after the samples were oven dried at 105 ºC for 24 h. Dry soil mass to core volume was calculated and bulk density was expressed as g/cm^3. The pycnometer method with distilled water as the displacement fluid was used to determine the particle density. Total porosity was calculated from bulk density (ρb) and particle density (ρp) using the following equation:

$$\text{Total porosity } (\%) = \left\{1 - \left(\frac{\rho b}{\rho p}\right)\right\} \times 100$$

Mineralogical characterization

X-ray diffraction (XRD): X-ray diffractometer was used to examine the structure and crystalline phases of the samples. Measurements were conducted with Cu$K\alpha$ radiation (wavelength = 1.5418 Å), scanning across angles from 20º to 80º to capture diffraction patterns.

Fourier transform infrared spectroscopy (FTIR): FTIR [Bruker Alpha, Lab India Instrument Private Limited] was used to investigate the molecular structure and bonding characteristics of minerals in the samples. FTIR spectroscopy spectra were recorded in transmittance mode within the wavenumber range of 3500-500 cm^{-1} and data were analyzed using OPUS 7.5 software.

Dynamic light scattering (DLS): The hydrodynamic size and zeta potential of the samples were measured using a Zeta-Sizer Nano ZS90 (Malvern Instruments) at 25 ºC. Samples were sonicated for 5 min prior to analysis to minimize aggregation. Data were processed using ZetaSizer 7.13 software.

Chemical analysis

pH measurement: The pH of the samples was measured in aqueous suspensions. For pH determination, a 1:2.5 ratio of sample to deionize water was prepared, shaken for 1 h and allowed to equilibrate for 30 min. The pH was measured using a calibrated digital pH meter.

Electrical conductivity measurement: Electrical conductivity was measured in a 1:5 sample to water extract after shaking for 1 h and filtering through Whatman No. 42 filter paper. The measurement was performed using a calibrated conductivity meter, with the results expressed in dS/m at 25 ºC after temperature correction.

Major elements analysis: The collected samples were analyzed for major elements (Si, Al, Fe, Ca, Mg, K, Na, Ti, P and Mn) using an ICP-OES technique by microwave digestion system. Digestion was achieved by the pouring of 10 mL of nitric acid (65% v/v) into 0.25 g homogenized sample into a Teflon vessel. The tightly closed vessel was then placed in a microwave digestion system with the process program containing up to 200 ºC at 45 bar pressure in 15 min and then constant at 200 ºC for 15 min followed by cooling step to the room

temperature for 30 min. The digested solution was then filtered with a Whatman filter after the cooling step. The solution was then transferred to a 50 mL volumetric flask and ultrapure water cooled to 4 ºC and the solution PTE analysis. The Argon plasma was used and the RF generator power was 0.7 to 1.7 kW. The plasma flow rate, auxiliary gas flow rate, nebulizer flow rate, coolant flow, sample pump speed and RR power were 13 L min^{-1}, 0.8 L min^{-1}, 0.8 L min^{-1}, coolant flow, 13 L min^{-1} and 1.2 kW, respectively. Solutions for ICP-OES calibration were made by diluting multielement standard stock solution (1000 mg L^{-1}). The PTE analysis was repeated three times. Weight percentages of the corresponding oxides (SiO_2, Al_2O_3, Fe_2O_3, CaO, MgO, K_2O, Na_2O, TiO_2, P_2O and MnO) were expressed as the results.

Trace element and heavy metal analysis: Trace elements and heavy metals (Zn, Pb, Cd, Cu, As, Cr, Ni, Co, V and others) were analyzed using inductively coupled plasma mass spectrometry (ICP-MS). The analysis was conducted on an Agilent 7900 ICP-MS instrument equipped with a collision/reaction cell to minimize spectral interferences.

Statistical analysis: Comparative analysis of soil and jarosite waste properties was conducted using Prism software. Correlation analysis was performed to identify relationships between different parameters. The statistical significance of correlations was assessed at the 95% confidence level ($p < 0.05$).

RESULTS AND DISCUSSION

XRD analysis: The XRD patterns of jarosite waste displayed characteristic diffraction peaks at 2θ values of 17.5º, 20.2º, 28.7º, 29.2º, 30.1º, 35.5º, 39.5º, 47.2º and 50.8º, which are consistent with the reference patterns of jarosite minerals [15]. The high intensity of these peaks indicates the crystalline nature of jarosite in the waste material [16]. Secondary phases identified in the jarosite waste included iron oxides (hematite and goethite) with peaks at 33.2º, 36.5º, 49.5º and 62.5º and minor amounts of quartz with peaks at 26.6º and 36.5º (Fig. 1) [17]. The presence of these secondary phases suggests partial transformation of jarosite minerals during the waste storage or aging process. The soil samples exhibited XRD patterns dominated by quartz (peaks at 26.6º, 20.8º, 36.5º, 39.4º, 42.4º, 45.8º, 50.1º and 54.9º) and clay minerals (peaks at 12.3º, 19.8º, 24.9º and 35.0º) [14]. Minor amounts of feldspars and calcite were also detected in the soil samples. The distinct XRD patterns between jarosite waste and soil samples confirm their different mineralogical compositions.

FTIR spectroscopic analysis: The FTIR spectral analysis of jarosite waste samples exhibited the characteristic absorption bands at 3400 cm^{-1} (OH *str.*), 1630 cm^{-1} (H-O-H bend.), 1190 and 1080 cm^{-1} (SO_4 *str.*), 800 cm^{-1} (Fe-OH def.) and 630 and 510 cm^{-1} (Fe-O *str.*) (Fig. 2). These absorption bands confirmed the occurrence of jarosite minerals in the waste material and correspond directly to the structural framework of jarosite [$KFe_3(SO_4)_2(OH)_6$] [18]. The observed broad band around 3400 cm^{-1} is ascribed to the stretching vibrations of the hydroxyl (OH) functional group involving both structural and adsorbed water present in the jarosite crystals lattice. This band is especially important because hydroxyl groups form a part of the jarosite

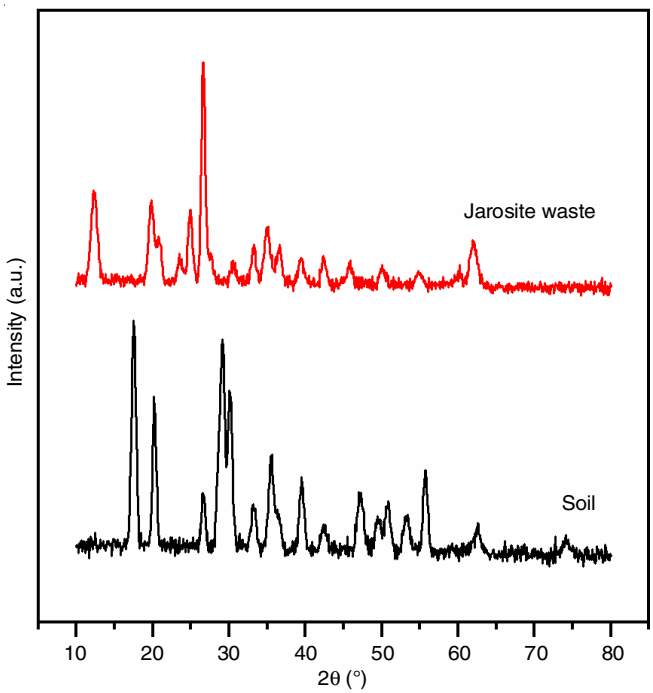

Fig. 1. XRD patterns showing characteristic diffraction peaks for jarosite minerals in waste samples (17.5º, 20.2º, 28.7º, 29.2º, 30.1º) compared to soil samples dominated by quartz (26.6º) and clay minerals

structure and they occupy certain crystallographic positions and help to maintain the stability of the mineral. The band at 1630 cm^{-1} is associated with bending vibrations of the H-O-H bonds in water, which means that there is both structural water and physically adsorbed moisture [19]. Absorption bands at 1190 and at 1080 cm^{-1} are especially diagnostic of SO_4^{2-} tetrahedral stretching vibrations and form the most significant spectral characteristics of jarosite minerals. Such bands are related to the asymmetric stretching vibration of sulfate groups that is the main anionic skeleton within the jarosite structure. The tetrahedral SO_4^{2-} ions are joined to the iron octahedral *via* oxygen atoms to form the three-dimensional structure that characterize jarosite minerals. This is confirmed by the existence of these characteristic bands of sulfate confirming that the crystal structure of the jarosite has been preserved in the waste product. The 800 cm^{-1} absorption band can be attributed to Fe-OH deformation vibrations and correspond to the bending of hydroxyl ligands linked to iron in the octahedral positions in the structure of jarosites. The band plays a pivotal role in determining the levels of iron-hydroxyl bonding structure which defines the jarosite minerals. The 630 and 510 cm^{-1} bands are attributed to Fe-O stretches in the iron octahedral units in the backbone of the jarosite structure, as they occur as corner sharing groups with the SO_4^{2-} tetrahedra. Such low-frequency vibrations are typical of iron-bearing minerals and so it has confirmed the octahedral coordination of Fe^{3+}. Conversely, the absorption bands in the soil samples were characteristic of the silicate minerals with intense Si-O stretching bands at 1030 cm^{-1} and strong Si-O-Al bending bands at 530 and 470 cm^{-1} [20]. The Si-O band of stretching indicates the basic mode of vibration of silicate tetrahedral, which are the basic

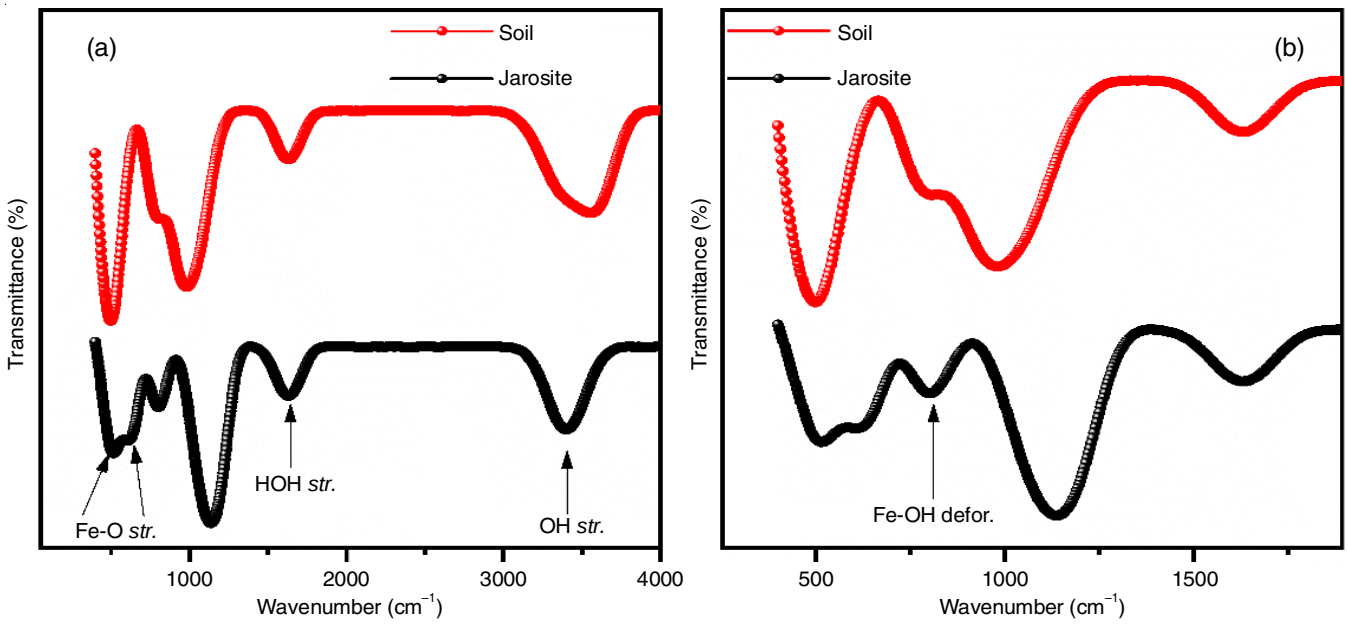

Fig. 2. FTIR spectra showing characteristic absorption bands for jarosite waste (sulfate stretching at 1190 and 1080 cm^{-1}, Fe-O stretching at 630 and 510 cm^{-1}) compared to soil samples dominated by silicate mineral features (a), enlarged FTIR spectra (b)

constituent of clay minerals and quartz that are abounded in soils. These Si-O-Al stretching motions reveal the presence of aluminosilicate minerals and the presence of aluminosilicate miner in the form of aluminum atoms replacing silicon atoms in the tetrahedral position creates the typical optical line of phyllosilicate clay minerals. The variations in the spectra of the FTIR of the jarosite waste and the soil materials are related to the different mineralogies and structural form of these two samples. Its jarosite waste is characterized by dominance of sulfate mineral structures containing iron-hydroxyl bonding and the soil samples are characterized by silicate-based mineralogy containing aluminum-silicon framework characteristics of natural weathering products.

Physical properties: The major physical properties of jarosite waste and nearby soil samples are shown in Table-1. The jarosite waste presented strong acidity, with pH levels between 2.6 and 3.3 significantly lower than the soil samples. The increased acidity levels found in jarosite minerals present significant environmental challenges, as they have the potential to leach and release harmful heavy metals into adjacent regions. The jarosite waste material also showed much higher electrical conductivity (3.57-4.58 mS/cm), roughly five- to six-folds higher than the soil (0.67-0.81 mS/cm), pointing to a heavy load of dissolved salts and ions. These values are similar to acid mine drainage from sulfide rich waste deposits [21]. The jarosite waste also surpassed the soil in bulk density with 1.81-2.01 g/cm^3 as compared to 1.23-1.37 g/cm^3 for soil, likely due to its iron-rich makeup and tightly packed structure [22]. The jaro-site waste consisted of much finer grains (39-49 µm) compared to the coarser soil particles (113-114 µm), which increases its specific surface area and may increase leaching of heavy metals [23]. Smaller particles provide with more surface area, which could speed up the leac-hing of harmful metals. Interestingly, despite its more refined texture, the waste

TABLE-1
PHYSICAL PROPERTIES OF JAROSITE WASTE AND SOIL SAMPLES

Sample	pH	EC (mS/cm)	Bulk density (g/cm^3)	Particle size (µm)	Moisture content (%)
JW-1	2.9	4.39	2.01	49	16.50
JW-2	2.6	4.37	1.93	47	24.20
JW-3	2.9	4.58	1.99	47	18.00
JW-4	3.0	3.94	1.81	43	18.60
JW-5	3.3	3.57	1.95	39	17.80
S-1	7.4	0.80	1.23	113	23.70
S-2	6.4	0.81	1.35	114	26.40
S-3	7.1	0.67	1.37	114	24.00

contained marginally less moisture (16.5-24.2%) compared to the soil (23.7-26.4%), potentially due to the water-repellent properties of specific jarosite minerals.

Zeta potential studies: The jarosite waste exhibited positive zeta potential values at pH < 3.2, with a maximum value of approximately +15 mV at pH 3.6. The isoelectric point (IEP) of jarosite waste was observed at pH 3.2, above which the zeta potential became increasingly negative, reaching approximately -25 mV at pH 6.2. The soil samples showed a different behaviour, with an IEP at approximately pH 5.8. The zeta potential of soil samples was negative at pH < 5.8, with values ranging from -20 mV at pH 2.0 to -2 mV at pH 3.6. Above pH 5.8, the zeta potential became positive, reaching a maximum of about +18 mV at pH 5.2, before decreasing again at higher pH values (Fig. 3). The lower IEP of jarosite waste compared to soil samples indicates its more acidic surface properties, which is consistent with the overall acidic nature of jarosite minerals.

The environmental implications of this zeta potential results are great as far as the mobility and transport behaviour of jarosite particles and heavy metals concerned. Jarosite waste particles

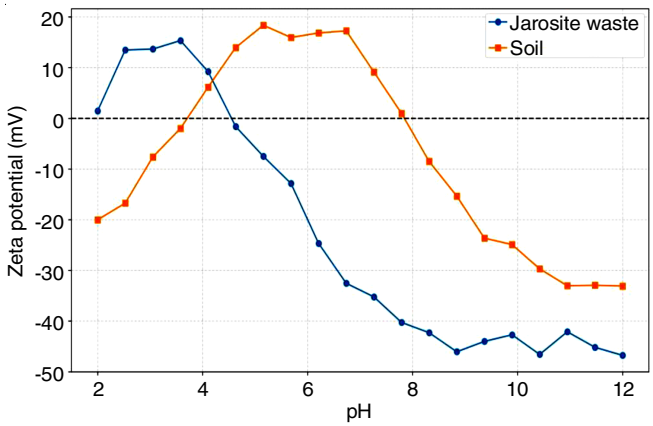

Fig. 3. Zeta potential measurements showing the pH-dependent surface charge properties of jarosite waste (isoelectric point at pH 3.2) and soil samples (isoelectric point at pH 5.8)

would clog up at a pH near 3.2 (IEP) because an increase in electrostatic attraction appealing to the formation of larger clusters of impurities and secondary minerals [24]. This flocculating action would decrease the mobility of jarosite particles in the groundwater systems and has the possibility of decreasing the short range dispersion of contaminated particles in the environment. Nevertheless, the bigger particles can be deposited quickly, which causes the locally concentrated collection of heavy metals in soil and sediments under discharging sites.

Major element analysis: The major elements composition of jarosite waste and soil samples is presented in Table-2. The jarosite waste samples (JW-1 to JW-5) exhibited significantly higher concentrations of Fe_2O_3 (37.82-42.54%), SO_3 (20.88-26.14%) and ZnO (6.05-7.69%) compared to the soil samples. This composition is consistent with the formation of jarosite minerals during zinc hydrometallurgical processing, where iron precipitation occurs in the presence of sulfate ions. The high iron and sulfate content confirms the predominance of jarosite minerals ($KFe_3(SO_4)_2(OH)_6$) in the waste material. In contrast, soil samples (S-1 to S-3) showed typical composition of natural soils with SiO_2 (63.10-64.23%), Al_2O_3 (13.41-14.79%) and Fe_2O_3 (7.00-7.56%) as the dominant components. The jarosite waste samples also contained the higher levels of PbO (0.82-1.02%), which is significantly higher than the concentrations found in soil samples (0.01%), which indicates the co-precipitation of lead during the jarosite formation process. The relatively low concentrations of CaO (2.11-2.37%), MgO (0.83-1.04%) and Na_2O (0.58-0.68%) in jarosite waste suggest the minimal incorporation of these elements in the jarosite structure. The K_2O content (3.26-4.58%) in jarosite waste is consistent with the potassium-bearing nature of jarosite minerals. The XRD analysis also confirmed that the waste material was rich in jarosite minerals with diffraction peaks characteristic of jarosite waste from zinc processing as reported by Kerolli-Mustafa *et al.* [25]. Secondary phases, such as iron oxides (hematite and goethite) are present which indicate the partial transformation of jarosite during storage, which was also reported by Paktunc & Dutrizac [17]. It could have occurred through dehydration and oxidation processes under different environmental conditions [26].

Trace elements and heavy metals analysis: The jarosite waste samples also contained extremely high concentrations of Zn (52,084-59,979 mg/kg), Pb (5,938-8,612 mg/kg) and Cd (140-237 mg/kg), which are orders of magnitude higher than those in the soil samples. These elevated concentrations reflect the incorporation of heavy metals during the jarosite precipitation process in zinc hydrometallurgy. Other potentially toxic elements such as Cu (848-1,057 mg/kg), As (353-538 mg/kg) and Cr (112-145 mg/kg) were also found at concerning levels in the jarosite waste (Table-3). The concentrations are far above the regulatory limits set by the different environmental agencies. For example, the Dutch Intervention Values for soil remediation set limits of 720 mg/kg for zinc, 530 mg/kg

TABLE-2
MAJOR ELEMENT COMPOSITION (WEIGHT %) OF JAROSITE WASTE AND SOIL SAMPLES

Sample	SiO_2	Al_2O_3	Fe_2O_3	CaO	MgO	K_2O	Na_2O	TiO_2	P_2O_5	MnO	SO_3	ZnO	PbO
JW-1	15.64	5.61	40.17	2.37	0.86	3.54	0.68	0.32	0.19	0.10	22.9	6.73	0.90
JW-2	13.74	5.36	40.60	2.11	1.04	3.76	0.58	0.38	0.22	0.11	23.48	7.61	1.02
JW-3	14.06	6.29	37.82	2.13	0.88	4.58	0.63	0.28	0.23	0.09	26.14	6.05	0.82
JW-4	16.04	6.45	40.52	2.15	0.90	3.26	0.58	0.30	0.23	0.11	20.88	7.69	0.90
JW-5	14.19	6.16	42.54	2.30	0.83	3.59	0.62	0.33	0.19	0.10	21.82	6.35	0.97
S-1	63.21	14.79	7.56	5.74	2.05	2.87	1.98	0.67	0.44	0.14	0.52	0.02	0.01
S-2	63.10	13.41	7.55	6.44	2.83	2.95	1.77	0.71	0.47	0.22	0.51	0.02	0.01
S-3	64.23	14.57	7.00	5.60	1.97	3.00	1.86	0.70	0.39	0.17	0.48	0.02	0.01

TABLE-3
TRACE ELEMENT AND HEAVY METAL CONCENTRATIONS (mg/kg) IN JAROSITE WASTE AND SOIL SAMPLES

Sample	Zn	Pb	Cd	Cu	As	Cr	Ni	Co	V	Ba	Sr	Rb
JW-1	56597	7636	237	975	436	129	67.7	44.8	85.8	438	175	99.3
JW-2	57698	5938	217	1057	470	112	115.0	35.5	92.5	425	153	86.9
JW-3	58867	6656	142	960	353	139	81.9	55.5	75.0	305	202	77.5
JW-4	59979	8612	140	976	436	145	77.4	36.1	91.7	334	187	99.9
JW-5	52084	7451	193	848	538	139	78.0	49.4	72.6	358	211	83.3
S-1	74	27	1	36	8	62	30.3	10.5	79.1	473	250	123.6
S-2	65	30	0	39	9	61	29.4	12.9	77.3	498	257	108.8
S-3	57	19	0	32	8	57	35.9	12.7	69.4	460	242	91.1

for lead and 13 mg/kg for cadmium [27]. Even lower thresholds are set by the Canadian Soil Quality Guidelines for the Protection of Environmental and Human Health of 200 mg/kg for zinc, 140 mg/kg for lead and 10 mg/kg for cadmium in residential areas [28]. The soil samples, in contrast, showed much lower concentrations of heavy metals, with Zn (57-74 mg/kg), Pb (19-30 mg/kg) and Cd (0-1 mg/kg) within typical background ranges for uncontaminated soils.

Correlation analysis: Correlation analysis was performed to identify the relationships between different parameters in jarosite waste samples. Fig. 4 shows the correlation matrix of key parameters. Strong positive correlations ($r > 0.7$) were observed between Fe_2O_3 and heavy metals (Zn, Pb and Cd), suggesting that iron oxides play a significant role in binding these metals in the jarosite structure. SO_3 content showed strong positive correlations with Zn ($r = 0.82$) and Pb ($r = 0.75$), indicating the co-precipitation of these metals with sulfate during jarosite formation. A strong negative correlation was observed between pH and EC ($r = -0.88$), which is consistent with the increased dissolution of minerals and release of ions under more acidic conditions. It was also shown that there are significant correlations between the physical properties and chemical composition. For example, bulk density was positively related to Fe_2O_3 and negatively related to particle size ($r = -0.65$ and $r = 0.71$ respectively). These correlations lead to understanding the governing factors of the physical behaviour of jarosite waste and its environmental impacts.

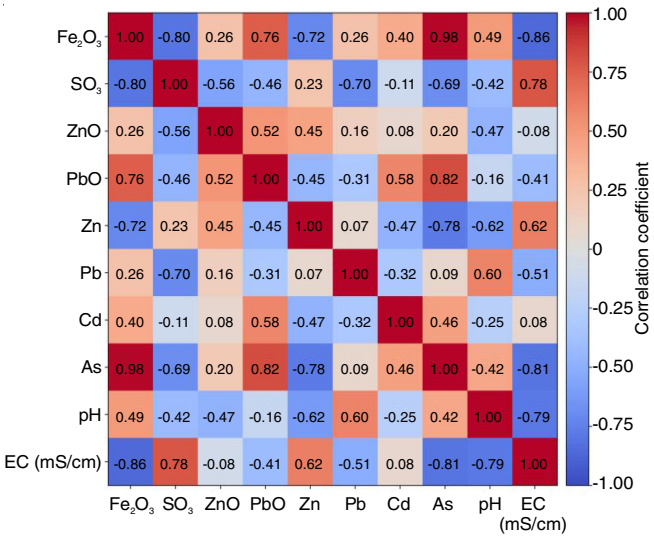

Fig. 4. Correlation matrix showing relationships between major elements, trace elements and physical properties in jarosite waste samples. Strong positive correlations ($r > 0.7$) were observed between Fe_2O_3 and heavy metals and between SO_3 and Zn/Pb concentrations

The incorporation of heavy metals into the jarosite structure can be due to the isomorphic substitution, adsorption and co-precipitation [29]. Dutrizac [30] stated that lead can substitute for potassium in the jarosite structure or zinc and cadmium can replace iron or adsorbed onto the mineral surface. This explains the strong correlations between Fe_2O_3, SO_3 and heavy metal concentrations [19]. Environmental behaviour of jarosite waste and natural soils also differs mineralogically. Properties such as water retention, cation exchange capacity and buffering capacity are affected by the predominance of jarosite minerals in the waste material as compared to the silicate dominated composition of natural soils. Also, the jarosite minerals have limited buffering capacity to pH changes that can further acidify the surrounding environments [31]. This clearly indicates that jarosite waste should be properly managed and remediated.

Remediation and management strategies: Heavy metal content and extreme acidity of the jarosite waste products define its interaction with the environment as an issue of concern that must be addressed *via* good management strategies. Lime and cement treatment is another method of stabilization that minimizes the metal leaching to create a stabilized derivative of jarofix [13]. In a study conducted by CSIR-CRRI through field trials in Rajasthan, jarofix was able to match or even produce superior results to conventional soil when used on road embankments or as a subgrade layer and little to no contaminant was released even after 2-3 years [32]. This application would facilitate the concepts related to a circular economy because waste is used to generate building materials.

Furthermore, research on the manganese-based perovskites highlights the potential for developing functional materials with photoluminescent properties from stabilized waste, opening new fields for the applications in smart ceramics or printing technologies [33]. This method is within the Indian standard requirements on the materials regarding subbase and the material can be used again in a long-term reuse process. Moreover, there is also a possibility of concrete paver blocks by replacing part of portland cement content with 10-15% jarofix, as the researchers of IIT Roorkee and other researchers have found that 10-15% jarofix replaces part of Portland cement, thereby reducing the amount of cement used and concrete paver block maintains its structural integrity [4]. In addition, studies on the temperature-responsive perovskites suggest that processed jarosite waste could be explored for applications in smart materials such as thermochromic coatings for energy-efficient windows [34,35].

Extraction by acid leach followed by reductive extraction produces value metals (*e.g.* zinc, lead, cadmium) and fertiliser raw materials (*e.g.* zinc nitrate), which is in accordance to waste to wealth paradigms [26]. Furthermore, investigations into the structural and electrical properties of lead-free materials suggest potential for repurposing stabilized waste derivatives in the advanced applications such as optoelectronic devices [36]. The practice of land reclamation by various zinc smelting industries has involved the admixture of mycorrhizal inoculation to Miyawaki afforestation and has reclaimed the loss of biodiversity on Jarofix waste disposal sites [13]. Such measures together with environmental monitoring could improve the management of jarosite waste and reduce its environmental impact, as emphasized by Peng *et al.* [2], thereby formulating a complicated solution to the challenge of managing jarosite waste with the minimal environmental repercussions.

Conclusion

This study characterizes jarosite waste generated from zinc hydrometallurgical processing in a comprehensive manner and

evaluates the environmental implications of this waste. Results show that jarosite waste has high iron, sulfur and heavy metal concentrations (*e.g.* zinc, lead and cadmium) exceeding limits for soil contamination. The mineralogical analysis shows that jarosite minerals are dominant and are accompanied by secondary iron oxide and quartz. Jarosite waste has strong environmental risks due to its extreme acidity and high electrical conductivity, as the physical properties of the waste are such that it will leach metals and generate acid. The comparison between jarosite waste and natural soils shows that this industrial waste has a high potential of contamination. The statistical analysis shows strong correlation between heavy metal concentrations and major components of jarosite waste, indicating co-precipitation mechanism for jarosite formation.

ACKNOWLEDGEMENTS

The authors sincerely thank Dr. Naresh Sharma for the help regarding characterization facility. One of the authors, Vaseem Akhtar, extends a special thanks to Miss Laxmi Paliwal (AGM HZL Vendanta Resources, Udaipur), Mr. Pradeep Singh (Head, Environment Department HZL Vendanta Resources, Udaipur) and Mr. Pardasarthi Chirapully (GM HZL Vendanta Resources, Udaipur) for all the help provided at their end.

CONFLICT OF INTEREST

The authors declare that there is no conflict of interests regarding the publication of this article.

REFERENCES

1. V.S. Litvinenko, *Nat. Resour. Res.*, **29**, 1521 (2020); https://doi.org/10.1007/s11053-019-09568-4
2. J. Peng, H. Liu, L. He, Z. Sun, Y. Peng, X. Huang and X. Yan, *Sustainability*, **15**, 9472 (2023); https://doi.org/10.3390/su15129472
3. K.M. Renaud, The Mineral Industry of India. Minerals Yearbook: Area Reports: International Review 2014 Asia and the Pacific, vol. 3 (2018).
4. P. Kushwaha, M. Agarwal and A. Ghosh, *Mater. Today Proc.*, **76**, 201 (2023); https://doi.org/10.1016/j.matpr.2022.12.178
5. L.G. Dyer, W.R. Richmond and P.D. Fawell, *Hydrometallurgy*, **119-120**, 47 (2012); https://doi.org/10.1016/j.hydromet.2012.02.017
6. M. Cruells and A. Roca, *Metals*, **12**, 802 (2022); https://doi.org/10.3390/met12050802
7. Z. Piervandi, A.K. Darban, S.M. Mousavi, V. Funari, M. Abdollahy, G. Asadollahfardi, E. Dinelli, R.D. Webster and M. Sillanpää, *Chemosphere*, **258**, 127288 (2020); https://doi.org/10.1016/j.chemosphere.2020.127288
8. L. Zhu, C. Lin, Y. Wu, W. Lu, Y. Liu, Y. Ma & A. Chen, *Environ. Geol.*, **53**, 1491 (2008); https://doi.org/10.1007/s00254-007-0758-y
9. M. Zhu, Y. Wang, C. Zheng, Y. Luo, Y. Li, S. Tan, Z. Sun, Y. Ke, C. Peng and X. Min, *J. Environ. Manag.*, **370**, 122396 (2024); https://doi.org/10.1016/j.jenvman.2024.122396
10. R. Pérez-López, A.M. Álvarez-Valero, J.M. Nieto, R. Sáez and J.X. Matos, *Appl. Geochem.*, **23**, 3452 (2008); https://doi.org/10.1016/j.apgeochem.2008.08.005
11. A. Navarro, E. Cardellach, J.L. Mendoza, M. Corbella and L.M. Domènech, *Appl. Geochem.*, **23**, 895 (2008); https://doi.org/10.1016/j.apgeochem.2007.07.012
12. F.M. Romero, M.A. Armienta and G. González-Hernández, *Appl. Geochem.*, **22**, 109 (2007); https://doi.org/10.1016/j.apgeochem.2006.07.017
13. Annual Report 2022-2023; Hindustan Zinc Limited, Hindustan Zinc Limited, Udaipur, India (2023).
14. H.E. Jamieson, S.R. Walker and M.B. Parsons, *Appl. Geochem.*, **57**, 85 (2015); https://doi.org/10.1016/j.apgeochem.2014.12.014
15. G.A. Desborough, K.S. Smith, H.A. Lowers, G.A. Swayze, S.F. Diehl, J.M. Hammarstrom, R.W. Leinz and R.L. Driscoll, *Geochim. Cosmochim. Acta*, **74**, 1041 (2010); https://doi.org/10.1016/j.gca.2009.11.006
16. M. Kerolli-Mustafa, L. Curkovic, H. Fajkovic and S. Ronèevic, *Croat. Chem. Acta*, **88**, 189 (2015); https://doi.org/10.5562/cca2554
17. D. Paktunc and J.E. Dutrizac, *Can. Mineral.*, **41**, 905 (2003); https://doi.org/10.2113/gscanmin.41.4.905
18. J. Majzlan, P. Drahota and M. Filippi, *Rev. Mineral. Geochem.*, **79**, 17 (2014); https://doi.org/10.2138/rmg.2014.79.2
19. S.A. Welch, D. Kirste, A.G. Christy, F.R. Beavis and S.G. Beavis, *Chem. Geol.*, **254**, 73 (2008); https://doi.org/10.1016/j.chemgeo.2008.06.010
20. Y. Wang, L. Jiao, C. Zhao, W. Dong, W. Gong and D. Dong, *Sci. Rep.*, **15**, 7678 (2025); https://doi.org/10.1038/s41598-025-90322-7
21. L. Alakangas, E. Andersson and S. Mueller, *Environ. Sci. Pollut. Res. Int.*, **20**, 7907 (2013); https://doi.org/10.1007/s11356-013-1838-z
22. E. Yilmaz, Gospodarka Surowcami Mineralnymi-Mineral Resources Management, **27**, pp. 89-112 (2011).
23. A. Qureshi, C. Maurice and B. Öhlander, *J. Geochem. Explor.*, **160**, 44 (2016); https://doi.org/10.1016/j.gexplo.2015.10.014
24. X. Wang, H. Zhao, L. Chang, Z. Yu, Z., Xiao, S. Tang, C. Huang, J. Fan and S. Yang, *ACS Omega*, **7**, 39169 (2022); https://doi.org/10.1021/acsomega.2c05067
25. M. Kerolli-Mustafa, H. Fajkovic, S. Ronèevic and L. Curkovic, *J. Geochem. Explor.*, **148**, 161 (2015); https://doi.org/10.1016/j.gexplo.2014.09.001.
26. A. Pappu, M. Saxena and S.R. Asolekar, *Sci. Total Environ.*, **359**, 232 (2006); https://doi.org/10.1016/j.scitotenv.2005.04.024
27. F.A. Swartjes, M. Rutgers, J.P. Lijzen, P.J. Janssen, A. Wintersen, P.F. Otte, E. Brand and L. Posthuma, *Sci. Total Environ.*, **427-428**, 1 (2012); https://doi.org/10.1016/j.scitotenv.2012.02.078
28. CEPA, National Guidelines and Standards Office, Quebec, Canada (2007).
29. K.A. Hudson-Edwards, *Mineral. Mag.*, **67**, 205 (2003); https://doi.org/10.1180/0026461036720095
30. J.E. Dutrizac, in eds.: R.G. Bautista, Hydrometallurgical Process Fundamentals. NATO Conference Series, Springer, Boston, MA, USA (1980).
31. P. Acero, C. Ayora, C. Torrentó and J.M. Nieto, *Geochim. Cosmochim. Acta*, **70**, 4130 (2006); https://doi.org/10.1016/j.gca.2006.06.1367
32. A. Pappu, M. Saxena and S.R. Asolekar, *Build. Environ.*, **42**, 2311 (2007); https://doi.org/10.1016/j.buildenv.2006.04.015
33. Dinesh and A. Sharma, *Ceram. Int.*, (2025); https://doi.org/10.1016/j.ceramint.2025.04.323
34. A. Sharma, V.K. Rao, D.V. Kamboj, R. Gaur, M. Shaik and A.R. Shrivastava, *New J. Chem.*, **40**, 8334 (2016); https://doi.org/10.1039/C5NJ03460D
35. Dinesh, *Ceram. Int.*, **51**, 23021 (2025); https://doi.org/10.1016/j.ceramint.2025.02.404
36. D. Kulhary and N. Dhariwal, *Mater. Sci. Eng. B*, **321**, 118552 (2025); https://doi.org/10.1016/j.mseb.2025.118552